IEEE Access
Multidisciplinary | Rapid Review | Open Access Journal

Received December 3, 2019, accepted February 13, 2020, date of publication February 18, 2020, date of current version March 2, 2020.

Digital Object Identifier 10.1109/ACCESS.2020.2974890

Adaptive Background Suppression Method Based on Intelligent Optimization for IR Small Target Detection Under Complex Cloud Backgrounds

XIANGYANG REN, (Student Member, IEEE), JIE WANG, TIANLEI MA, CAITONG YUE, (Student Member, IEEE), AND KE BAI
School of Electrical Engineering, Zhengzhou University, Zhengzhou 450000, China

Corresponding author: Tianlei Ma (tlma@zzu.edu.cn)

This work was supported in part by the National Natural Science Foundation of China under Grant 61903340, in part by the Postdoctoral Science Foundation of Henan Province under Grant 001701002, in part by the Key Scientific Research projects of universities in Henan under Grant 19A413002, and in part by the Project of Young Talent Promotion of Henan Association for Science and Technology under Grant 2020HYTP028.

ABSTRACT To improve the detection of dim and small targets in infrared (IR) images containing high-intensity cloud clutter, a novel adaptive background suppression method is proposed. By using three-dimensional cooperative filtering and differential calculation, the different and complex background clutter is suppressed. To obtain the optimal parameters for the background suppression algorithm, an adaptive parameter optimization method is proposed. The adaptive parameter optimization problem is transformed into a multiobjective optimization problem in which the signal-to-clutter ratio gain and background suppression factor, which effectively reflect the background suppression performance, are chosen as the optimization objectives, and the parameters of the proposed background suppression algorithm are considered as the variables. To effectively solve the established multiobjective optimization problem, a particle swarm parameter optimization-based method is utilized. Experimental results indicate that the proposed adaptive background suppression method using these optimal parameters has good performance for IR images in real complex scenes, as well as performance superior to that of other baseline methods.

INDEX TERMS Background suppression, infrared (IR) images, three-dimensional cooperative filtering, multiobjective optimization algorithm.

I. INTRODUCTION

Detecting small targets from IR images with complex backgrounds is a challenging task [1], [2]. Since the targets are far from the IR detection systems, their shapes and construction features are not available. In addition, the intensity of the background clutter, such as cloud clutter, is much higher than the noise caused by the sensor, even higher than the intensity of the dim and small targets that need to be detected [3], [4]. To improve the detection performance for dim and small targets in complicated backgrounds with high-intensity cloud clutter, an effective IR clutter background suppression method is critical.

In general, IR image background suppression methods are classified into three types [5]: methods based on a spatial filter [6]–[11], methods based on a temporal filter [12]–[16] and methods based on the frequency domain [8], [17]–[19]. The methods based on a spatial filter usually operate on pixels in a sliding window. In these methods, the background pixels are assumed to be spatially correlated and the target pixels are different from them, such as in the Max-Mean/Max-Median filter method [6], the two-dimensional least mean square (TDLMS) filter method [7], the nonparametric regression-based method [8], the bilateral filter [9] and other human visual system-based methods [10], [11]. The predicted IR image background can be acquired by different spatial filters. The background-suppressed image is obtained by subtracting the predicted IR image background of the original image. However, when a background with complicated clutter is constantly changing, these methods generally have a high false-positive rate.

The associate editor coordinating the review of this manuscript and approving it for publication was Ravibabu Mulaveesala.

Unlike the spatial filter-based methods operating on pixels in a sliding window, methods based on a temporal filter typically utilize background trajectory features to suppress the complicated background in the temporal domain [12], [13]. In this sort of method, the background pixels are assumed to be stationary in the temporal domain, while the pixels of the dim and small target are assumed to be nonstationary; examples of these methods include temporal difference projection [14], infinite impulse response [15] and the triple temporal filter [16]. These methods can achieve good background suppression performance under some circumstances. However, the background suppression performance for IR images obtained for real scenes is significantly reduced because the background of successive frame images is typically not stationary.

Furthermore, many researchers have proposed a number of methods based on the frequency domain that have good background suppression performance [17], [18]. Transform domain methods first use Fourier [8], wavelet [19] or other transforms to convert the IR image into the frequency domain and then suppresses the background by removing the low-frequency subband while preserving the target shape and energy. Finally, background suppression of the IR image is achieved by inverse transformation. Although frequency domain-based methods have access to global resources, these methods do not effectively suppress a complicated background when the edges of the background clutter are decomposed into a high-frequency subband.

In addition to the above three categories, some methods treat background suppression as a unique denoising process because they assume that a small target in an IR image can be assimilated into a rare impulse noise [20], [22], [25]; an example of such a background suppression detection method is called detection by nonlocal means (D-NLM) [20]. The nonlocal means (NLM) filter is a denoising algorithm based on the principles of local regularity and self-similarity [21]. D-NLM depends on the same principles as the NLM filter to search for similar local blocks, and an improved measure is applied to robustly estimate backgrounds despite the presence of small targets. On the basis of [20], a novel method based on the block matching and 3D filtering technique (BM3D) and a Gaussian mixture matched filter (GMMF) was proposed [4]. This method (DBM3D+GMMF) estimates the background mean based on the output of a BM3D filter, which is one of the most efficient denoising algorithms [23], [24]. Although these methods have excellent background suppression performance, since the temporal information is not utilized, the small targets may be suppressed along with the complicated background clutter. In contrast to the DBM3D+GMMF method, Hu *et al.* [25] first used a modified NLM algorithm and designed a new weight calculation model based on a circular mask to estimate the image background. Then, the temporal information between adjacent frames was utilized to achieve background suppression. Although these methods that treat background suppression as a unique denoising process have good background suppression performance, they only utilize similar block information in a single frame image or time information between adjacent images. In addition, some of the parameters in these algorithms are set empirically and cannot be adaptively set based on image information. Therefore, when background clutter is complex and constantly changing, it is difficult for these methods to accurately estimate the background.

To make full use of the spatiotemporal information in the image sequence and adaptively select the parameters of the background suppression algorithm, a new adaptive background suppression method is proposed. In our method, we treat the small target to be detected as a rare impulse noise and use the spatiotemporal information in the image sequence to suppress complex background clutter. This method takes advantage of three-dimensional cooperative filtering and differential calculation to achieve background suppression. Considering the subjectivity of the artificial adjustment of background suppression algorithm parameters, we transform the parameter selection problem into a multiobjective optimization problem to get the adaptive algorithm parameters. In a multiobjective optimization problem, we take the parameters of the proposed background suppression method as the variables and the signal-to-clutter ratio gain (G_{SCR}) and the background suppression factor (BSF) of the background suppression method as the optimization objectives. Then, a method based on particle swarm parameter optimization is used to obtain the optimal parameters of the background suppression algorithm.

The contributions of this research are summarized as follows:

1) An adaptive background suppression algorithm is proposed. The optimization algorithm is utilized to obtain the optimal parameters of the background suppression algorithm.
2) For the optimization algorithm can not be effectively applied to the practical problem, a local optimization strategy is given in the adaptive background suppression algorithm.

Section II of this paper gives the IR image model. In Section III, the detailed background suppression method is explained. The formulation of a problem of optimizing adaptive parameters is given in Section IV. Section V shows the method of selecting adaptive parameters. Section VI presents the experiments and analysis. Conclusions are drawn in section VII.

II. IR IMAGE MODEL

In general, an IR image acquired in a cloudy area can be assumed to consist of three components. These are the background component, the noise component, and the target component. The IR image can be modeled as:

$$I(x, y) = T(x, y) + B(x, y) + N(x, y) \tag{1}$$

where $T(x, y)$ represents the target component, $B(x, y)$ denotes the background component, and $N(x, y)$ is the noise component.

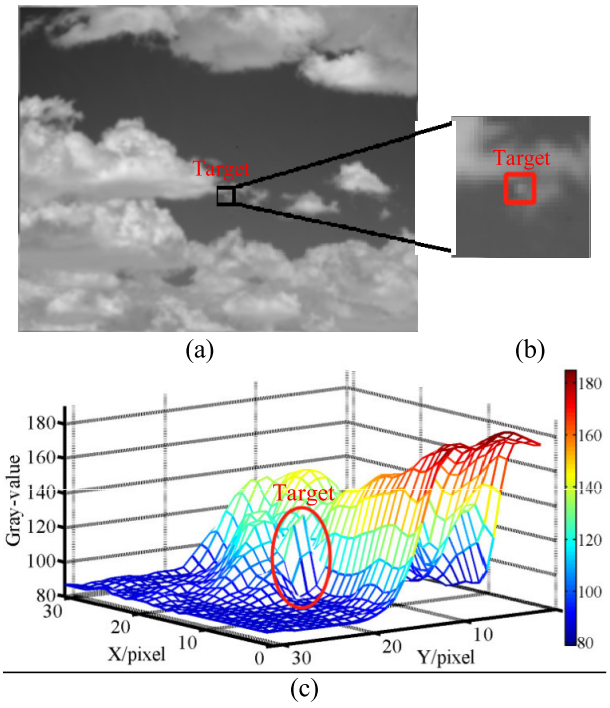

FIGURE 1. Representative IR image of small target and complex background.

A dim and small target component $T(x, y)$ usually occupies only a few pixels in an IR image [47]. A representative small target and complex background are given in Fig. 1. Fig. 1 (a) shows a small target on a complicated background, Fig. 1 (b) shows a magnified view of the target, and Fig. 1 (c) illustrates the 3D intensity distribution of the small target and the complicated background.

Considering that the shapes of the small targets in IR images radiate from a center and have features similar to those of two-dimensional (2D) Gaussian functions, many scholars take advantage of the point spread function model to model dim and small targets [42]. These targets can be modeled as follows:

$$f_T(x, y) = A \cdot \exp\left\{-\frac{1}{2}\left[\frac{(x - x_c)^2 + (y - y_c)^2}{s^2}\right]\right\} \quad (2)$$

where $f_T(x, y)$ denotes the small target, A represents the peak intensity, (x_c, y_c) is the position of the target center, and s denotes the σ in the Gaussian function [10].

The $N(x, y)$ in the image is considered to be independent and subject to the Gaussian random distribution of $N(0, \sigma^2)$ [42], [46].

The $B(x, y)$ in the IR image can be divided into two states [14]:

(a) Sky: This is area A in Fig. 2. Although the change in this area is relatively flat, the clutter source in this area is mainly noise.

(b) Cloud: In general, cloud clutter can be separated into two parts, the interior of the cloud and the edge of the cloud, which are represented as area B and area C in Fig. 2.

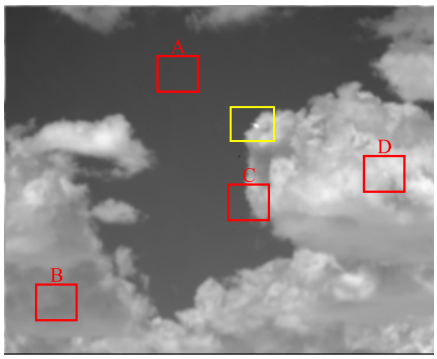

FIGURE 2. An IR image with complicated cloud clutter. The red squares represent the background of the different states and the yellow square is a small target.

As the external environment changes, for example, due to changes in meteorological conditions, the intensity of the cloud constantly changes. In addition, the cloud clutter also includes regions of abnormally high intensity, as shown by area D in Fig. 2. Due to the specific solar incident angle and the anomalous distribution of ice particles in the cloud, the intensity of this region is significantly higher than those of other regions, with a shape similar to that of the small target.

III. PROPOSED IR IMAGE BACKGROUND SUPPRESSION METHOD

In this section, first, the inspiration for the proposed method is described. Then, a cloud clutter suppression method using spatiotemporal information in an image sequence is introduced. Finally, a noise suppression method is given.

A. THE INSPIRATION FOR THE PROPOSED METHOD

Since IR images in the same sequence are acquired by the same IR detector and the sampling interval of the image sequence is very short, the image backgrounds of successive frames are similar. A set of continuous IR images with a complex background is given in Fig. 3.

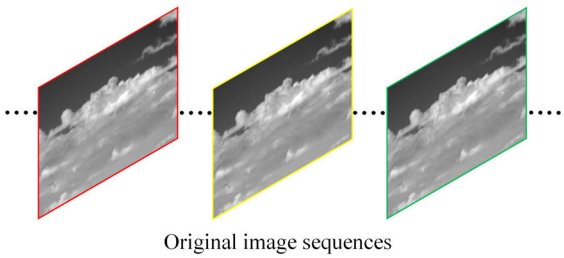

FIGURE 3. An IR image sequence for a real scene.

In our method, as in methods in the related literature [20], [22], [25], the small target is regarded as a rare impulse noise, and the background suppression method is also considered to be a unique denoising process. In the related literature, the information from similar blocks in a single frame image and the temporal information between adjacent images are

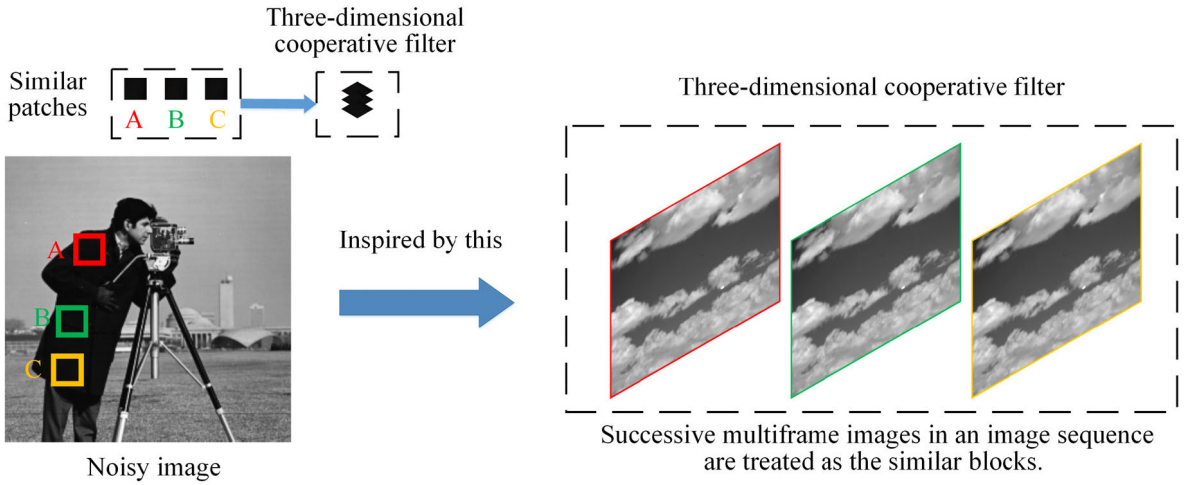

FIGURE 4. The inspiration for the three-dimensional cooperative filter in our method.

utilized for background suppression. Inspired by these methods, first, successive multiframe images are treated as similar blocks in our method. Then, these similar blocks are filtered by three-dimensional cooperative filtering.

Three-dimensional cooperative filtering is a step in the BM3D algorithm [23]. The BM3D algorithm performs well compared with other algorithms in the field of image denoising. In a BM3D filter, many of the most similar patches in an image are first searched and then sorted into different groups. The noise in the different groups is then suppressed by cooperative filtering. Finally, all similar denoised blocks are weighted, and the denoised image is obtained.

The inspiration process of the three-dimensional cooperative filter in our method is given in Fig. 4. It can be seen that the BM3D filter first searches for similar patches in an image and then filters those patches with three-dimensional cooperative filtering [23], [24]. The image of the person with a camera is a noisy image from [23]. Inspired by the related works [20], [22], [25] and the BM3D filter, in our method, successive multiframe images in an image sequence are first treated as similar blocks, and then these similar blocks are filtered by three-dimensional cooperative filtering.

After filtering these consecutive multiframe images, the images that only contain $B(x, y)$ and $N(x, y)$ are obtained via the original image and the corresponding filtered difference calculation. The complicated cloud background of the images is suppressed through this process.

B. THE CLOUD CLUTTER SUPPRESSION METHOD

Unlike the method of constructing the 3D matrix of similar blocks in the BM3D filter, the 3D image matrix used in our method is integrated by continuous frame images, because these continuous images have a similar background.

The 3D image matrix $M_o^{r\times c\times N_f}$ is composed of continuous original images, where $r \times c$ denotes the size of these images, and N_f denotes the frame of the images. After $M_o^{r\times c\times N_f}$ is integrated, the 2D image blocks in $M_o^{r\times c\times N_f}$ are transformed to the frequency domain using a 2D Fast Fourier Transform (FFT). Then, the third dimension of $M_o^{r\times c\times N_f}$ is digitally transformed using a 1D FFT. After the two FFTs, the transformed $M_o^{r\times c\times N_f}$ is hard thresholded. Specifically, the coefficients in the transformed $M_o^{r\times c\times N_f}$ that are smaller than the cooperative hard threshold $\Upsilon(\cdot)$ will be defined to zero. Finally, the 3D image matrix $M^{r\times c\times N_f}$ processed by three-dimensional cooperative filtering is acquired after the 1D Fast Fourier inverse transform and the 2D Fast Fourier inverse transform of the 3D matrix. The expression for the filtering process is given in Eq. (3):

$$M^{r\times c\times N_f} = \mathbb{F}^{-1}\left(\Upsilon\left(\mathbb{F}\left(M_o^{r\times c\times N_f}\right)\right)\right) \tag{3}$$

where $\mathbb{F}^{-1}(\cdot)$ denotes the 1D inverse FFT and the 2D inverse FFT. $\mathbb{F}(\cdot)$ stands for the 1D FFT and the 2D FFT. $\Upsilon(\cdot)$ denotes a collaborative hard-thresholding for xx; it can be expressed as:

$$\Upsilon(xx) = \begin{cases} xx, & otherwise \\ 0, & if\ |xx| \le T \end{cases} \tag{4}$$

where T is the filter threshold.

After $M_o^{r\times c\times N_f}$ is processed by three-dimensional cooperative filtering, the cloud clutter-suppressed image is obtained by using a differential calculation between the filtered image and its corresponding original image. This process can be described as:

$$I_{cs}(i) = I(i) - I_f(i) \tag{5}$$

where $I_f(i)$ is the ith frame image after the three-dimensional cooperative filtering on $M^{r\times c\times N_f}$, $I(i) \in M_0^{r\times c\times N_f}$ denotes the corresponding original image of $I_f(i)$, and $I_{cs}(i)$ represents the cloud clutter-suppressed image.

These images, which contain only the noise component, are obtained by filtering the continuous multiframe images

and by the differential calculation. The small target, assumed to be a rare impulse noise, is included in the noise component of the image. The complicated cloud clutter can be suppressed through this process.

C. NOISE SUPPRESSION FOR THE CLOUD CLUTTER-SUPPRESSED IMAGE

After cloud clutter suppression, only noise and a small part of the single frame image are left. Since the noise in the images is subject to the distribution of $N\left(0, \sigma^2\right)$, after stacking N_f frame sequence images and performing mean filtering on them, the standard deviation σ of the noise will become $\sqrt{\sigma^2/N_f}$. The process of stacking and averaging filtering on multiframe images can suppress image noise.

The process of stacking N_f continuous frames I_{cs} can be expressed as:

$$I_{ac} = \sum_{n_t=0}^{N_f-1} I_{cs}\left(n_t\right) \tag{6}$$

where I_{ac} denotes the stacked image and $I_{cs}\left(n_t\right)$ represents the $n_t th$ cloud clutter-suppressed image.

Then, mean filtering is applied to the stacked image I_{ac}. This process can be expressed as:

$$I_{am} = I_{ac}/N_f \tag{7}$$

where I_{am} both denotes the cloud clutter-suppressed image after image noise suppression and represents the final image with background suppression.

After stacking and mean filtering on the successive multiframe cloud clutter-suppressed images, the noise of I_{am} is reduced to $1/\sqrt{N_f}$ of the noise of I. This process achieves image noise suppression, which can be expressed as:

$$I : N_I\left(x, y\right) \sim N\left(\mu, \sigma^2\right) \tag{8}$$

$$I_{am} : N_{I_{am}}\left(x, y\right) \sim N\left(\mu, \sigma^2/N_f\right) \tag{9}$$

where μ and σ represent the gray mean and standard deviation of the neighboring area, respectively.

The background suppression method is considered to be a unique denoising process in the proposed method, and small targets are taken as a rare impulse noise in each image. The complex cloud background clutter of the IR image is first suppressed by three-dimensional cooperative filtering and differential calculation. Then, stacking and mean filtering are applied to the images with cloud clutter background suppression. Finally, the background suppression of the IR image is realized. The proposed method is described in Algorithm 1, where $\mathbb{F}_{2D}\left(\cdot\right)$ denotes the 2D FFT and $\mathbb{F}_{1D}\left(\cdot\right)$ represents the 1D FFT. Similarly, $\mathbb{F}_{2D}^{-1}\left(\cdot\right)$ denotes the 2D inverse FFT, and $\mathbb{F}_{1D}^{-1}\left(\cdot\right)$ is the 1D inverse FFT. $\mathbb{F}\left(I_{mid}\right)$ denotes the result of performing $\mathbb{F}_{2D}\left(\cdot\right)$ and $\mathbb{F}_{1D}\left(\cdot\right)$ on I_{mid}, and $I_{mid} \in M_0^{r\times c\times N_f}$

Algorithm 1 Method for Suppressing Complex Background Clutter

Input: N_f continuous frames of IR images.
Output: Background-suppressed images.
1: Apply $\mathbb{F}_{2D}\left(\cdot\right)$ and $\mathbb{F}_{1D}\left(\cdot\right)$ to $M_0^{r\times c\times N_f}$.
2: Perform $\Upsilon\left(\cdot\right)$ on $\mathbb{F}\left(I_{mid}\right)$.
if $\left(\left|\mathbb{F}\left(I_{mid}\right)\right| \le T\right)$
set $\mathbb{F}\left(I_{mid}\right)$ to 0;
else set $\mathbb{F}\left(I_{mid}\right) = \mathbb{F}\left(I_{mid}\right)$
end if
4: Obtain $I_f\left(i\right) \in M^{r\times c\times N_f}$ via $\mathbb{F}_{2D}^{-1}\left(\cdot\right)$ and $\mathbb{F}_{1D}^{-1}\left(\cdot\right)$.
5: Use differential calculation on $I_f\left(i\right)$, and obtain the cloud clutter-suppressed images I_{cs}.

$$I_{cs}\left(i\right) = I\left(i\right) - I_f\left(i\right)$$

6: Stack the N_f frame cloud clutter-suppressed images.

$$I_{ac} = \sum_{n_t=0}^{N_f-1} I_{cs}\left(x, y, n_t\right)$$

7: Perform mean filtering on the stacked image I_{ac}.

$$I_{am} = I_{ac}/N_f$$

8: Obtain the background-suppressed image I_{am}.

IV. FORMULATION OF THE PROBLEM OF OPTIMIZING ADAPTIVE PARAMETERS

In the proposed IR image background suppression method, there are two parameters, the number of frames N_f and the filter threshold T, which are mutually constrained. It is assumed that the background suppression algorithm parameters obtained by manual adjustment are not optimal and are subjective. Therefore, to acquire the optimal parameters, we use an adaptive method to select parameters and transform the adaptive parameter selection method into a multiobjective optimization problem.

A. VARIABLES

In this multiobjective optimization problem, there are two variables: the number of frames N_f and the filter threshold T of the proposed background suppression algorithm.

The number of frames N_f is a crucial parameter. Its size has an impact on the computational complexity and background suppression performance of the background suppression method. As N_f increases, more interframe spatiotemporal information is used, which means the background suppression performance is improved, however the computational complexity of the algorithm increases. As N_f decreases, the computational complexity of the proposed method decreases; however, the background suppression performance of the algorithm also decreases.

The filter threshold T in our method determines the performance of cloud clutter background suppression. When T is

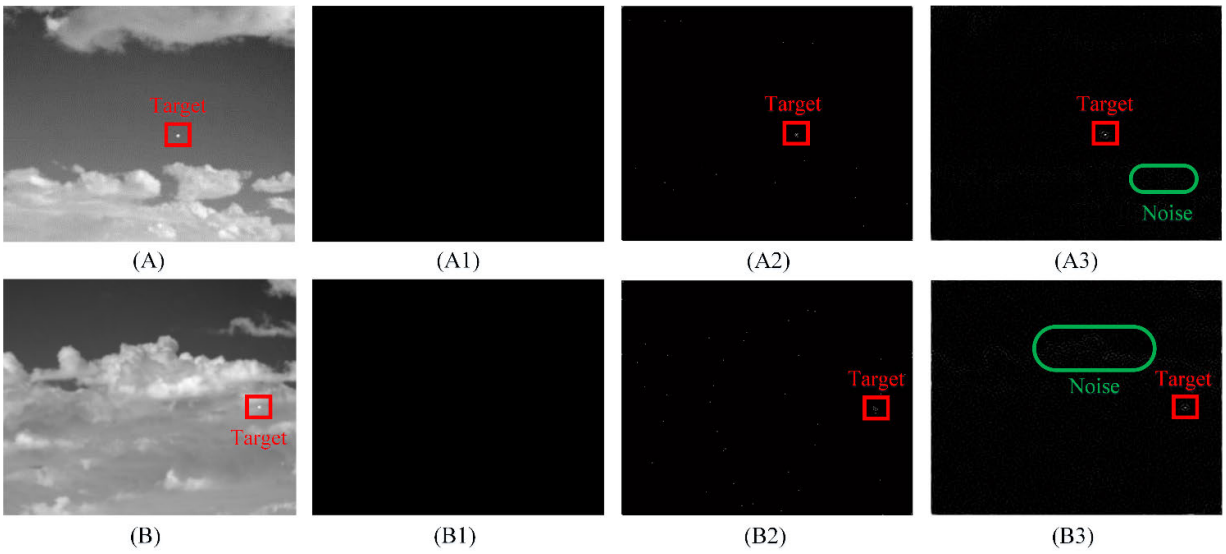

FIGURE 5. The background suppression results of two real image sequences. The dim target is represented by the red rectangle, and a representative example of residual noise is represented by the green oval.

smaller, $B(x, y)$ and $N(x, y)$ will not be filtered out. When choosing an appropriate T, the images of cloud clutter background suppression will only contain $N(x, y)$ and part of $B(x, y)$. When T is larger, there will be a large amount of residual background clutter in the filtered images. The experimental results based on two sets of IR image sequences are shown in Fig. 5. The representative images in each IR image sequence are presented in the first column of Fig. 5. Each frame includes complex backgrounds and a small target, and the size of each frame is 256 × 318 pixels. The background suppression results obtained by filtering the two image sequences using different thresholds are shown in the three columns on the right side of Fig. 5. In Fig. 5, (A) and (B) are representative frames from two real image sequences and (A1) and (B1) denote the resulting images when the threshold is $T = 80$. (A2) and (B2) are the resulting images when $T = 110$. (A3) and (B3) denote the resulting images when $T = 140$.

The optimal algorithm parameters are based on the premise that our method has optimal background suppression performance. However, the size of N_f and the size of T in our method influence each other, so we use an optimization algorithm to get the most appropriate algorithm parameters. In the optimization algorithm, the two parameters N_f and T are considered as variables and are optimized to obtain optimal background suppression performance. Each variable in the background suppression algorithm has its own bounds, which can be expressed as:

$$\begin{cases} N_{\min} \le N_f \le N_{\max}, \quad N_f \in N^* \\ T_{\min} \le T \le T_{\max} \end{cases} \tag{10}$$

where $[N_{\min}, N_{\max}]$ and $[T_{\min}, T_{\max}]$ denote the bounds on the size of N_f and the size of T in the background suppression method, respectively. N^* is the set of positive integers.

B. OPTIMIZATION OBJECTIVES

To objectively evaluate the background suppression performance, we use two metrics, G_{SCR} and BSF. They are the most commonly used indicators [50]. And they are also important indictors to final detection performance [51]. These metrics not only objectively reflect the performance of different background suppression methods but also indicate their target enhancement abilities. The larger the values of G_{SCR} and BSF, the more easily small targets are detected [50], [51].

The definition of G_{SCR} is as follows:

$$G_{SCR} = \frac{SCR_{out}}{SCR_{in}} \tag{11}$$

where SCR_{in} is the signal to clutter ratio of the images before background suppression, and SCR_{out} is the signal to clutter ratio of the images after background suppression. The SCR is defined as follows:

$$SCR = \frac{|\mu_t - \mu_b|}{\sigma_b} \tag{12}$$

where μ_t and μ_b denote the average pixel value in the target area and the neighboring area, respectively. In addition, σ_b is the standard deviation of the neighboring area. As shown in Fig. 6, a is the width of the small target, and b is the length of the small target. We set $d = 15$ [46].

BSF is another evaluation metric, and it can be defined as:

$$BSF = \frac{C_{in}}{C_{out}} \tag{13}$$

where C_{in} represents the standard deviation of the images before background suppression, and C_{out} represents the standard deviation of the images after background suppression.

Because these two metrics can effectively reflect the performance of the background suppression algorithm, they are

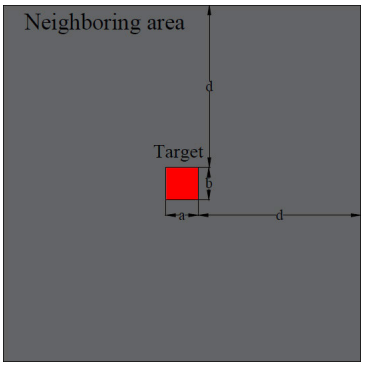

FIGURE 6. A small target and its neighboring area.

used as the optimization objectives for the optimization algorithm. After optimizing the variables, the maximum BSF and maximum G_{SCR} values of the IR images are obtained.

The parameter selection problem can be transformed into a multiobjective optimization problem, and the optimization objectives can be established as:

$$\begin{cases} \max obj_{GSCR} = \max\left(\frac{|\mu_t^{out}-\mu_b^{out}|}{\sigma_b^{out}} \cdot \frac{\sigma_b^{in}}{|\mu_t^{in}-\mu_b^{in}|}\right) \\ \max obj_{BSF} = \max\left(\frac{C_{in}}{C_{out}}\right) \end{cases} \tag{14}$$

where obj_{GSCR} and obj_{BSF} denote G_{SCR} and BSF, respectively.

C. THE LOCAL OPTIMIZATION STRATEGY

In the adaptive background suppression algorithm, the values of BSF and G_{SCR} are selected as the objectives of optimization. In contrast to the BSF value obtained from the gray value change of the whole image, the value of G_{SCR} is obtained by numerical calculation on a certain point and its neighboring area in the IR image. An ideal point for obtaining the maximum G_{SCR} value is a small target point. However, the position of the small target in the IR image is uncertain when calculating the value of the G_{SCR} in the optimization algorithm. Therefore, we present a novel local optimization strategy to select the appropriate point for the largest G_{SCR} value.

Since the characteristics of the small target accord with the point spread function model, our local optimization strategy is to find a point in the whole image that fits the point spread function model and optimize the filter algorithm parameter corresponding to the point. This process is actually equivalent to optimizing a small target, because the optimized point and the small target have characteristics that satisfy the point spread function model. The Laplacian of Gaussian (LOG) filter can be used to detect signals that conform to the point spread function model. In reference [10], the LOG filter is used to detect small targets. The LOG filter is defined:

$$LOG(x, y, s) = \frac{1}{\pi s^4}\left[1 - \frac{x^2+y^2}{2s^2}\right] e^{-\frac{x^2+y^2}{2s^2}} \tag{15}$$

Therefore, we applied the LOG filter to the original IR images. The process of using the LOG filter can increase the signal intensity of the target and the points having the same features as the target. After the filtering process, the maximum point spread function value in the image is found, and the coordinates corresponding to this value are utilized to obtain the maximum G_{SCR} value.

Using this strategy in the optimization algorithm, even if we do not know where the real target is, we can obtain the point that is consistent with the small target features and use that point to get the maximum G_{SCR} value, which is equivalent to the optimization of the real target. The proposed local optimization strategy is described in Algorithm 2

Algorithm 2 Method for Selecting the Point for the Largest GSCR Value

Input: The original IR images.

Output: The coordinates of the appropriate point for calculating the maximum G_{SCR} value.

1: Apply the LOG filter on the original IR images M_{ori}.

$$M_{LOG} = L_{OG}(M_{ori})$$

2: Obtain the LOG filtered image M_{LOG}.

3: Find the maximum value max (M_{LOG}) in M_{LOG}.

4: Get the coordinates of the max (M_{LOG}) point in the image.

5: Use the coordinates to calculate the maximum G_{SCR} value.

V. ADAPTIVE PARAMETER SELECTION METHOD

In the filtering algorithm, the setting of the algorithm parameters is often crucial [26]. Since the algorithm parameters cannot be adaptively changed according to the processing object, the performance of the algorithm will be degraded [27]. For example, in threshold parameter settings, hard and soft thresholds are commonly used, but they may easily cause image distortion [27], [28]. Therefore, attention has been drawn to exploring adaptive filtering methods. With the development of evolutionary algorithms, more and more denoising algorithms use evolutionary algorithms to obtain adaptive filtering methods [29]. In particular, the particle swarm optimization (PSO) algorithm is commonly utilized, because it has the characteristics of fast convergence and easy implementation [33]. Therefore, many adaptive filtering algorithms were proposed based on PSO [37]–[42]. These methods are widely used in different fields to denoise satellite cloud images [38], speech signals [39], electromagnetic radiation field signals [40], electroencephalogram signals [41], and so on; they have excellent denoising performance.

In our method, to achieve adaptive selection of filter parameters, a PSO algorithm is used. In this section, we first give a brief introduction to the PSO algorithm, then describe the concept of Pareto optimality and the procedure of the knee point selection method. Finally, the algorithm for the adaptive

parameter selection method based on MO_Ring_PSO_SCD is given.

A. A BRIEF INTRODUCTION TO THE PSO ALGORITHM

To better present the basic idea of the adaptive filtering algorithm based on the intelligent algorithm in parameter selection, we first briefly describe the PSO algorithm. The PSO algorithm is based on a population, and it can be modeled by the social behavior of birds within a flock [34], [35]. It is able to solve multiobjective optimization problems and is especially effective. First, a particle is initialized with a position vector and a random velocity. In this method, the historically best position of the particle is represented as p_{best}, and the historically best position of its neighborhood is denoted by n_{best}. At each iteration, in accordance with p_{best} and n_{best}, the particle's position is updated from the starting position to a better area. The update for each particle in the swarm is based on the following equations:

$$\vec{x}_i(t) = \vec{x}_i(t-1) + \vec{v}_i(t) \tag{16}$$

and

$$\vec{v}_i(t) = \omega\vec{v}_i(t-1) + C_1 r_1(\vec{x}_{pbest_i} - \vec{x}_i(t)) + C_2 r_2(\vec{x}_{nbest_i} - \vec{x}_i(t)) \tag{17}$$

where $\vec{v}_i(t)$ is the velocity of the tth generation's particle p_i, $\vec{x}_i(t)$ represents the position of particle p_i in the tth generation, r_1 and r_2 denote uniformly generated random values, C_1 and C_2 are constants utilized to stabilize exploration and exploitation processes, and ω is the inertia weight.

In our previous work, a new multiobjective particle swarm optimization algorithm with ring topology and a special crowding distance was proposed, which was abbreviated as MO_Ring_PSO_SCD. In this method, first, the personal best archive (PBA) and the neighborhood best archive (NBA) are built, and then p_{best} and n_{best} are selected from PBA and NBA. Multiple niches are induced by the designed ring topology. The results of testing on eleven multimodal and multiobjective test functions demonstrate that the algorithm outperforms other algorithms in decision space distribution. For more details about the MO_Ring_PSO_SCD method, please refer to [36].

In this paper, considering that the proposed background suppression method is a practical problem, there is no specific mathematical model for this problem, and it is difficult to define the problem as a single-mode problem. Therefore, in order to guarantee the diversity of the obtained background suppression method parameters, the MO_Ring_PSO_SCD method—which can effectively solve multimodal, multiobjective problems—is applied to select the optimal parameters for the background suppression filtering algorithm. The application of the MO_Ring_PSO_SCD method in the selection of background suppression algorithm parameters is described in Algorithm 3.

Algorithm 3 The MO_Ring_PSO_SCD-Based Adaptive Parameter Selection Method

1: Select the parameters N_f and T of the background suppression algorithm and provide a constraint range for these parameters, as described in Section IV.
2: Initialize the population and the number of particles M; then, determine the acceleration coefficients (C_1 and C_2) and inertia weight W.
3: Select BSF and G_{SCR} as the fitness function, and assess the fitness values of each particle.
4: Update the position and velocity of each particle according to Eq. (16) and Eq. (17).
5: Update PBA and NBA.
6: Determine whether the number of evaluations has reached the maximum
  if (the number of evaluations has reached the maximum)
    Terminate the iteration process;
  else
  Return to Step 3.
  end if
7: Get the final PS.
8: Select the final result by using the knee point selection method.
9: Obtain the optimal background suppression parameters N_f and T corresponding to the final result.

B. THE CONCEPT OF PARETO OPTIMALITY

In contrast to a single-objective optimization problem, the solution set of a multiobjective optimization problem contains several different global solutions. Before choosing the appropriate global solution, some crucial definitions often utilized in multiobjective optimization problems need to be introduced [44].

Generally, a multiobjective optimization problem that includes m objectives can be expressed as:

$$Min F(x) = (f_1(x), f_2(x), \ldots, f_m(x)) \tag{18}$$

Definition 1 (Pareto Dominance): When the solution x satisfies the condition of Eq. (19), it is said to dominate another solution z. This condition can be written as $x \succ z$.

$$\forall k \in \{1, 2, \ldots, m\}, f_k(x) \leq f_k(z), \quad \wedge \exists k, f_k(x) < f_k(z) \tag{19}$$

Definition 2 (Pareto-Optimal Set): If no other solution z satisfies $z \succ x$, then the solution x is called a Pareto-optimal solution. A Pareto-optimal set (PS) is composed of all the Pareto-optimal solutions.

Definition 3 (Pareto Front): The Pareto-optimal front PF denotes the mapping of the PS in the objective space. The PF can be expressed as:

$$PF = \{F(x) | x \in PS\} \tag{20}$$

C. THE PROCEDURE FOR THE KNEE POINT SELECTION METHOD

Considering that the parameter selection method based on the MO_Ring_PSO_SCD method is a multiobjective optimization algorithm, its solution set includes several different Pareto-optimal solutions. However, for IR image background suppression algorithms, one solution should be chosen from the *PS*. In addition, the background suppression method needs to perform better at enhancing the target signal and suppressing the background; that is, it needs G_{SCR} and *BSF* to have larger values at the same time. Better performance better enables the proposed background suppression method for small target detection systems.

In general, the knee point in *PF* is considered to be the best choice for the solution. The knee point selection method used in this paper is the distance to the extreme line method [45]. Because the point with the largest corner is to slightly improve the point where one target will cause deterioration of another target, this special critical point is chosen as the knee point.

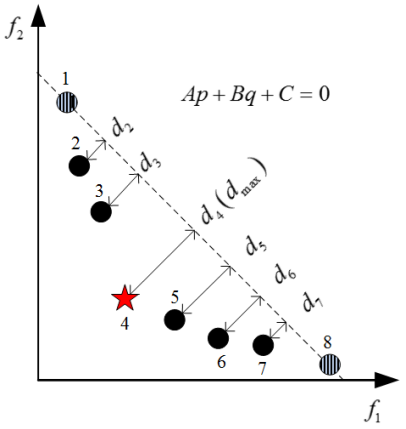

FIGURE 7. The distance to the extreme line method. The red star (point 4) is the knee point.

The process for the distance to the extreme line method is shown in Fig. 7. First, two extreme points are selected, namely, point 1 and point 8 in Fig. 7, since point 1 and point 8 have the maximum values in the objective functions f_1 and f_2, respectively.

Then, the extreme line is determined from the coordinates of the two extreme points. The limit line can be defined as:

$$Ap + Bq + C = 0 \tag{21}$$

where A, B, C, p and q are the parameters of the extreme line.

Finally, as given in Eq. (22), the distance from each point on the *PF* to the limit line is obtained, and the point with the largest distance is selected as a knee point.

$$d_i = \frac{|Ap_i + Bq_i + C|}{\sqrt{A^2 + B^2}} \tag{22}$$

where d_i denotes the distance.

D. THE MO_RING_PSO_SCD-BASED ADAPTIVE PARAMETER SELECTION METHOD

After briefly introducing the multiobjective optimization problem constructed in this paper, the MO_Ring_PSO_SCD algorithm and the knee point selection method, we summarize the application of the MO_Ring_PSO_SCD algorithm in adaptive parameter selection for the background suppression algorithm, as follows:

In summary, this paper uses an intelligent optimization algorithm to optimize the parameters of the background suppression algorithm and thereby obtain the optimal parameters in different sequences and the best background clutter suppression performance. The framework of the proposed adaptive background suppression method is shown in Fig. 8.

VI. EXPERIMENTS AND ANALYSIS

In this section, we first present the experimental images and baseline methods. Then, the settings of parameters are discussed. Finally, the effectiveness and practicability of our method are proved by using experimental images.

A. EXPERIMENTAL IMAGES AND BASELINE METHODS

The real IR image sequences used in our paper are obtained by an IR detector. The relevant information about the IR detector is listed in Table 1. There are eight sets of IR image sequences that are utilized as experimental images. These images contain a complicated cloudy background and a dim target. The details of the eight sequences are displayed in Table 2. The size of these images is 256 × 318 pixels. The representative images for these eight image sequences are illustrated in Fig. 10.

TABLE 1. Related information on the IR detector.

Focal length	The range of spectral	The field of view	Frame Frequency	The size of pixel
46 mm	3.7-4.8 μm	8°×11°	50 Hz	30 μm×30 μm

To prove the robustness of our proposed method, we utilize some baseline methods, including the Max-Mean and Max-Median methods [6], the TDLMS method [7], Kim's method [10], the 3DCF method [46], and the DBM3D+GMMF method [22]. The principal parameter settings of the different baseline methods are shown in Table 3.

B. THE SETTINGS OF PARAMETERS

1) THE PARAMETER SETTINGS FOR THE OPTIMIZATION METHOD

In the multiobjective optimization method, the range of the uniformly generated random values r_1 and r_2 is [0, 1]. The constants C_1 and C_2 are used to ensure a balance between the exploration and the exploitation processes. We set $C_1 = C_2 = 2.05$ in our paper. The inertia weight ω is set to 0.7298. The settings for these parameters in the multiobjective optimization method are the same as those in references

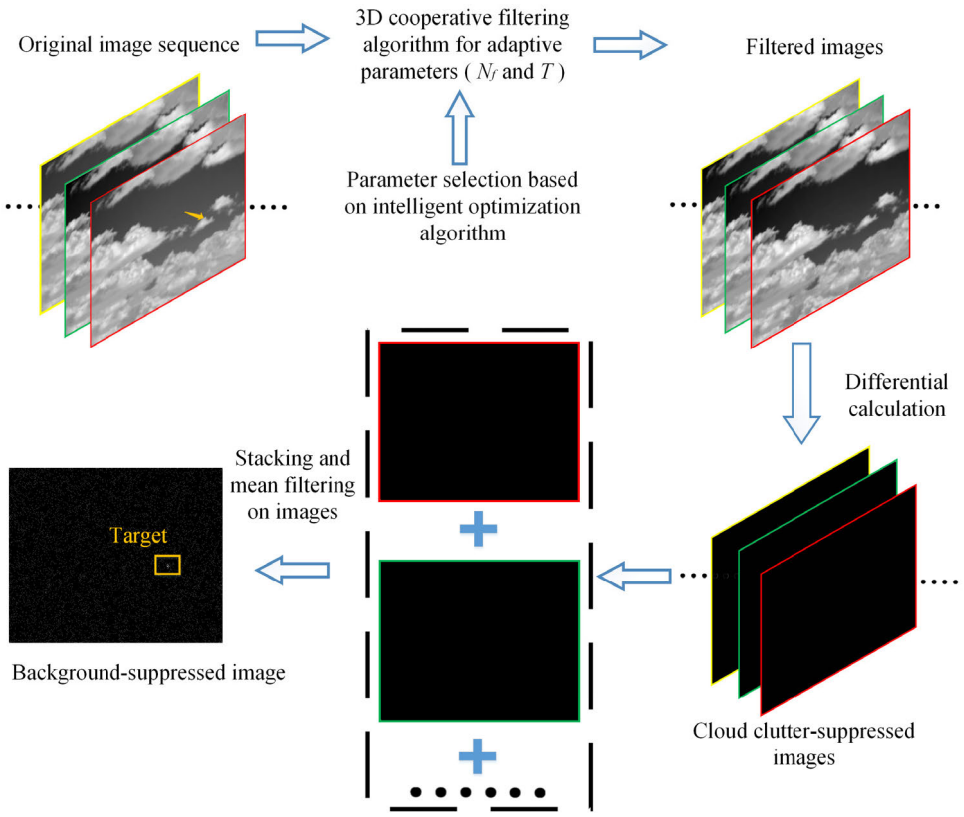

FIGURE 8. The flowchart for the adaptive background suppression method. The orange rectangle indicates the target.

TABLE 2. The details of the eight IR image sequences.

	# frame	The details of the target	The details of the background
Seq. 1	100	1. Target category: airplane 2. Target size: 2×2 pixels to 4×4 pixels.	1. Background type: Sky scene. 2. Clutter type: Cloud clutter.
Seq. 2	100	1. Target category: airplane 2. Target size: 2×2 pixels to 4×4 pixels.	1. Background type: Complex, changing sky scene. 2. Clutter type: Multilayer cloud clutter.
Seq. 3	100	1. Target category: airplane 2. Target size: 2×2 pixels to 3×3 pixels.	1. Background type: Complex, changing sky scene. 2. Clutter type: Multilayer, changing cloud clutter. Includes multiple abnormally high intensity cloud regions.
Seq. 4	100	1. Target category: airplane 2. Target size: 3×3 pixels to 5×5 pixels.	1. Background type: Complex sky scene 2. Clutter type: Multilayer, changing cloud clutter.
Seq. 5	100	1. Target category: airplane 2. Target size: 3×3 pixels to 4×4 pixels.	1. Background type: Complex sky scene. 2. Clutter type: Multilayer, changing cloud clutter.
Seq. 6	100	1. Target category: airplane 2. Target size: 2×2 pixels to 3×3 pixels.	1. Background type: Nonsmooth and nonuniform sky scene. 2. Clutter type: Multilayer, changing cloud clutter. Includes multiple abnormally high intensity cloud regions.
Seq. 7	150	1. Target category: airplane 2. Target size: 2×2 pixels to 3×3 pixels.	1. Background type: One part is a nonsmooth and nonuniform sky scene, and the other part is composed of mountains and buildings. 2. Clutter type: One part is multilayer, changing cloud clutter that includes multiple abnormally high intensity cloud regions. The other part is clutter generated by mountains and buildings, including some high-intensity regions.
Seq. 8	150	1. Target category: airplane 2. Target size: 3×3 pixels to 5×5 pixels.	1. Background type: One part is a complex sky scene, and the other part is a signal tower. 2. Clutter type: One part is complex cloud clutter, including some high-intensity cloud regions. The other part is the clutter generated by the signal tower, including some high-intensity regions.

[35], [36], [43], [48], [49]. Based on our previous work [46] and the complexity of the optimization algorithm, N_f is constrained to [2, 9], and T is constrained to [60, 140].

Through the proposed local optimization strategy, we can acquire some points as targets and use them to obtain the value of G_{SCR} in the optimization algorithm. The positions of

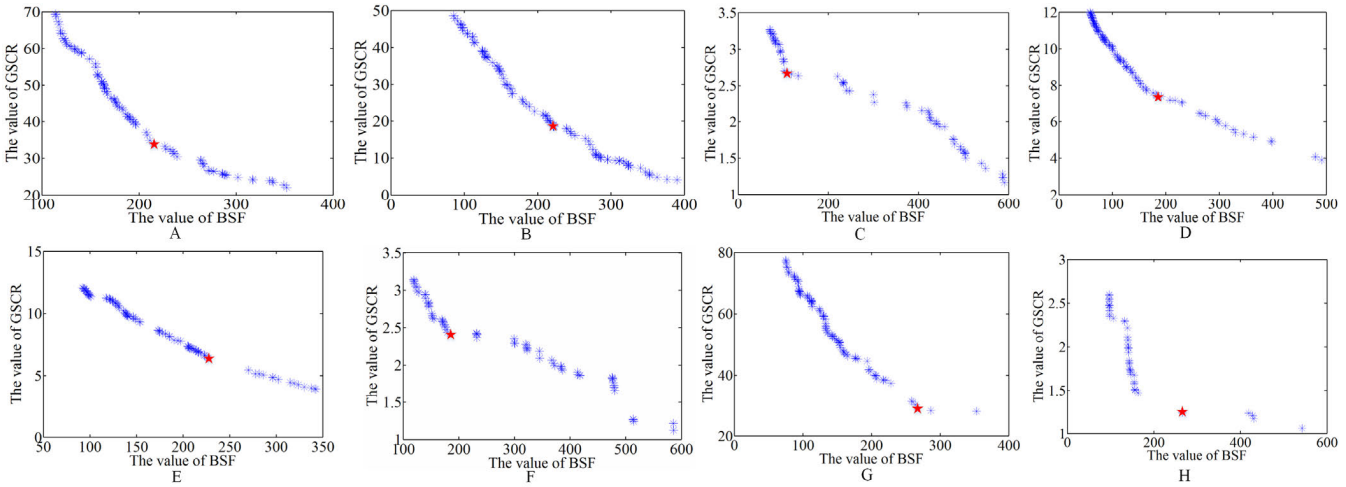

FIGURE 9. The *PF* of eight experimental image sequences processed by the multiobjective optimization algorithm. A- H in the figure denote the *PF* corresponding to image sequence 1 through image sequence 8, respectively. The red stars denote the selected points.

TABLE 3. The principal parameter settings of the different baseline methods.

Baseline method	The principal parameter settings of this method
Max-Mean method	The size of the filter: 15×15 pixels.
Max-Median method	The size of the filter: 15×15 pixels.
TDLMS method	The step size of the TDLMS: 1.0×1.0^{-6}. The number of quantization bits: 8. The number of image frames used in a single run: 5 frames.
Kim's method	The number of Laplacian scale-space images: 12. The range of the scale: $[0.6,6]$.
3DCF method	The number of frames: 9. The size of the filter threshold is set to twice the average value of the filtered image.
DBM3D+GMMF method	The number of classes: 7. The number of pixels per class: 5×9^2 pixels. The size of the threshold: 1.0×1.0^{10}.

these points in eight experimental image sequences are shown in Table 4. (mm, nn) denote the coordinates of the points.

2) THE PARAMETER SETTINGS FOR THE BACKGROUND SUPPRESSION ALGORITHM

In this section, to prove the effectiveness of the designed multiobjective optimization model, N_f and T are obtained for different image sequences according to the multiobjective optimization model. Here, eight sets of image sequences with different complex backgrounds are considered, and each sequence is tested by an evolution process with 100 initial particles and 50 iterations. The more suitable solution is selected from the *PF* obtained by the evolution process of the multiobjective optimization algorithm. The PFs of the optimal solutions for the eight experimental image sequences are shown in Fig. 9.

On the basis of the method of the distance to the extreme line, and the principle that the selected knee point corresponds to a smaller N_f, these knee points are selected; the background suppression algorithm parameters corresponding to the selected points are also given in Table 5. The value of G_{SCR} in the table is the value calculated from the point obtained by LOG filter.

It can be seen from the N_f and T corresponding to the selected points that some of the eight different image sequences have relatively large N_f values, indicating that the image background of these sequences is more complicated. These image sequences also have smaller values of G_{SCR} and *BSF* obtained by the optimization algorithm than image sequences with smaller N_f values.

C. CONTRAST EXPERIMENTS

After selecting N_f and T for the different image sequences, the background suppression performance of the proposed method is compared with these different baseline methods. According to Table 2, the eight experimental image sequences in the contrast experiment have different background features, including the image noise level and the intensity of the background clutter, so the difficulty of background suppression varies for different image sequences. Fig. 10 shows the background suppression results for different background suppression methods; these background-suppressed images come from eight different IR image sequences. From these figures, we can see that our method has better background suppression performance than the comparison algorithms in different complex backgrounds. In addition, there is more background clutter residual in the results of the Max-Mean method, the Max-Median method, Kim's method and Shao's method. Moreover, the DBM3D+GMMF method, the 3DCF method and the TDLMS method achieve better clutter suppression performance, especially in image sequence 4.

TABLE 4. The Position of the points in eight experimental image sequences.

	Seq. 1	Seq. 2	Seq. 3	Seq. 4	Seq. 5	Seq. 6	Seq. 7	Seq. 8
Position	(182, 192)	(138, 193)	(229, 238)	(226, 131)	(245, 148)	(255, 36)	(110, 248)	(20, 61)

TABLE 5. The selected points in the PF for the eight experimental image sequences.

	Seq. 1	Seq. 2	Seq. 3	Seq. 4	Seq. 5	Seq. 6	Seq. 7	Seq. 8
G_{SCR}	34.13	22.61	2.66	7.20	6.44	2.43	28.56	1.24
BSF	215.43	195.82	106.87	207.58	227.53	179.20	279.73	266.21
N_f	3	4	5	2	2	5	5	6
T	94.13	82.78	135.12	127.85	101.98	103.72	138.51	95.03

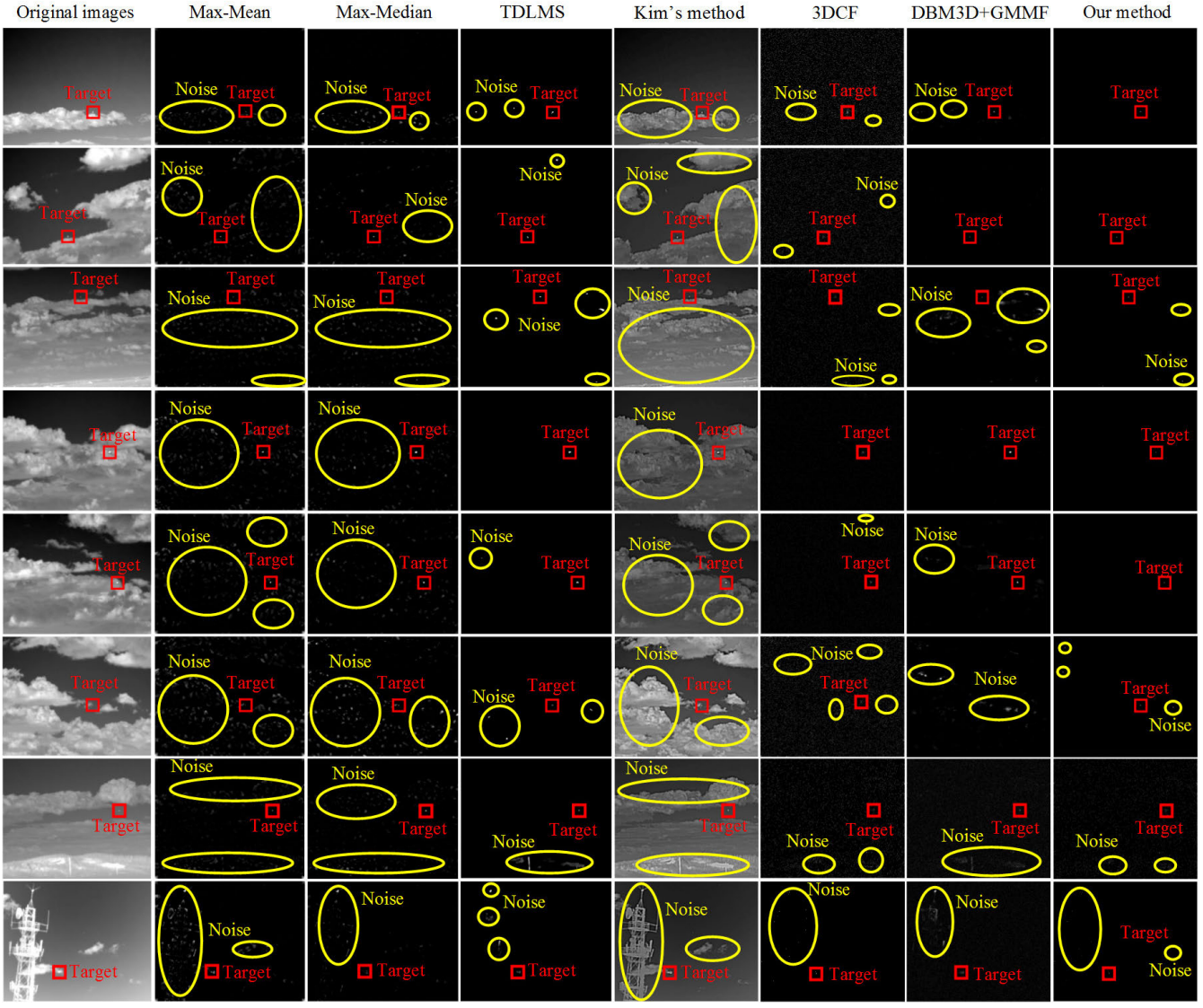

FIGURE 10. Background suppression results of different methods for eight IR image sequences. The first column shows the representative frame of each of the eight sequences. The dim target is represented by the red rectangle, and the representative example of noise is indicated by a yellow circle.

To further compare the background suppression performance of the different algorithms, the 3D intensity distribution of the background suppression results for the different algorithms in Fig. 10 are illustrated in Fig. 11. We can see from Fig. 11 that image sequence 4 and image sequence 5 have stronger target intensity and lower background complexity. Different background suppression methods have the least residual noise and the best background suppression per-

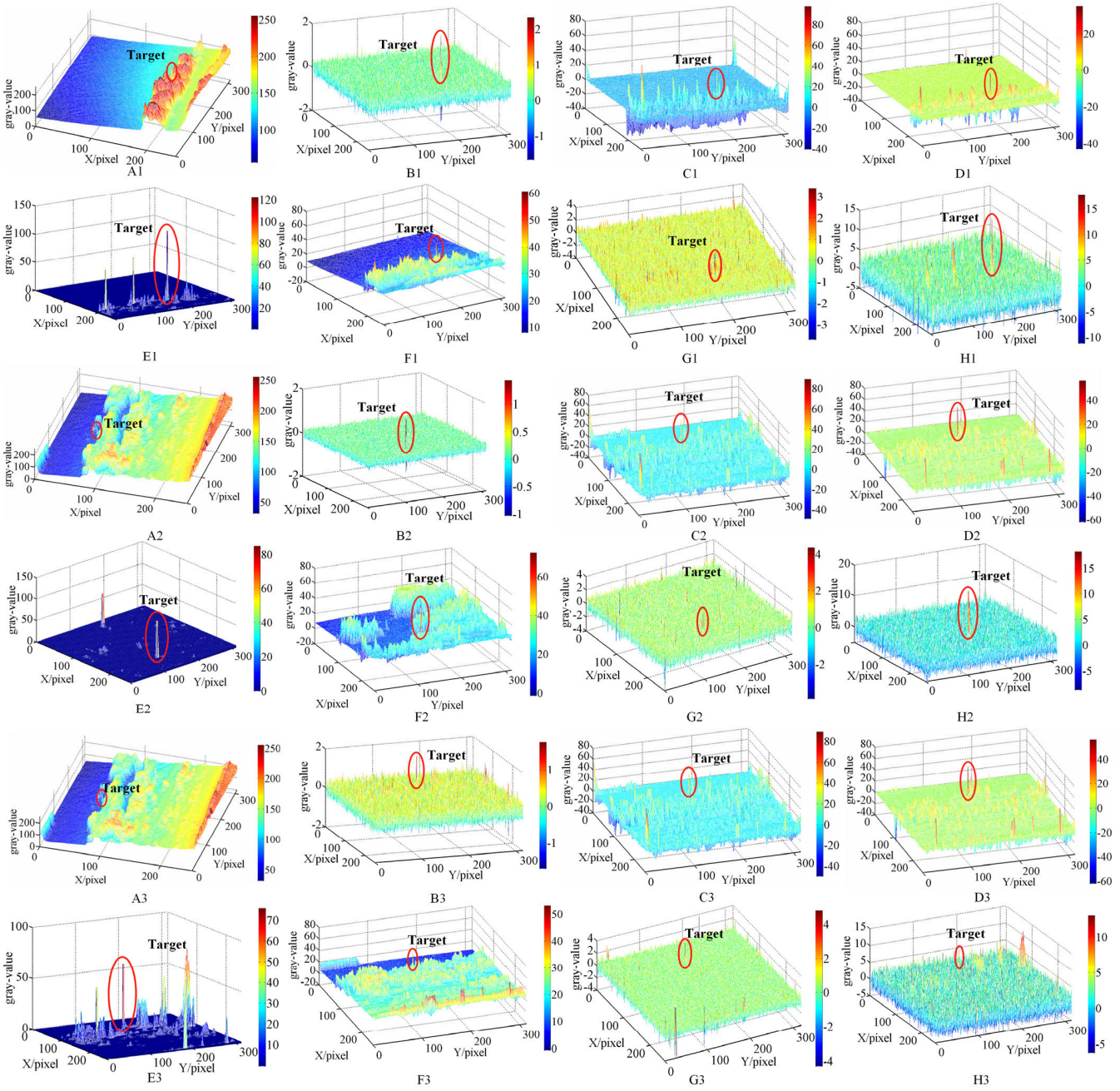

FIGURE 11. The 3D intensity distribution of the background suppression results of different methods for eight IR image sequences. A1-A8 denote the 3D intensity distribution of the representative frames of the eight experimental image sequences, respectively. B1-B8 represent the 3D intensity distribution of the results of our method in the eight image sequences, respectively. C1-AC represent the 3D intensity distribution of the results of the Max-Mean method in the eight image sequences, respectively. D1-D8 represent the 3D intensity distribution of the results of Max-Median method in the eight image sequences, respectively. E1-E8 represent the 3D intensity distribution of the results of the TDLMS method in the eight image sequences, respectively. F1-F8 represent the 3D intensity distribution of the results of Kim's method in the eight image sequences, respectively. G1-G8 represent the 3D intensity distribution of the results of the 3DCF method in the eight image sequences, respectively. H1-H8 represent the 3D intensity distribution of the results of the DBM3D+GMMF method in the eight image sequences, respectively. The small targets are indicated by red ovals.

formance for these images. At the same time, the target intensity of image sequence 1 and image sequence 2 is moderate, and their background complexity is also moderate. Therefore, different background suppression methods have less residual noise and better target enhancement performance in these image sequences. Furthermore, image sequence 3, image sequence 6, image sequence 7, and image sequence 8 have lower target intensity and higher background complexity. Therefore, in these four image sequences, the baseline methods have more residual noise and worse background suppression performance. Although the background complexity varies for different image sequences, our proposed method

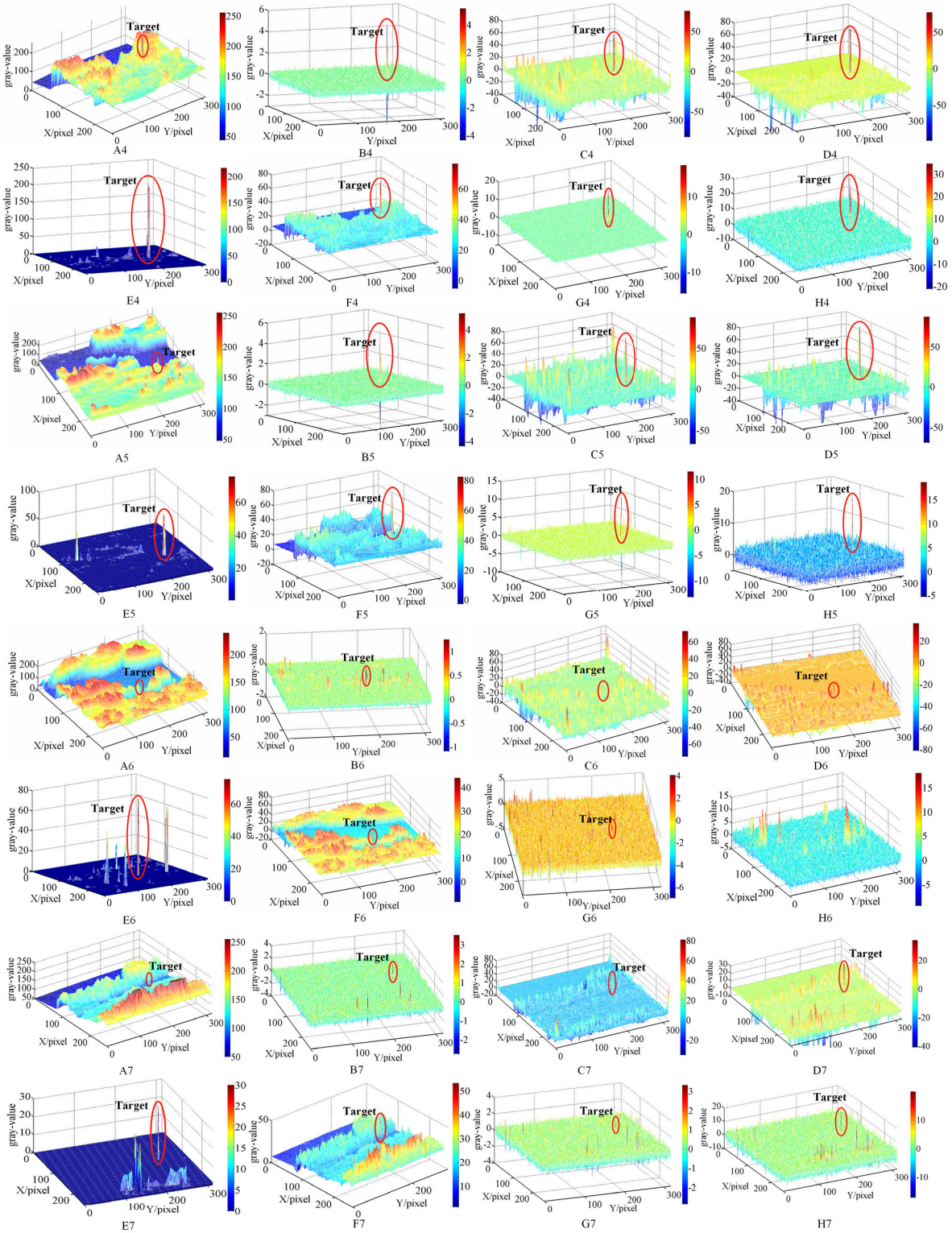

FIGURE 11. ***(Continued.)*** **The 3D intensity distribution of the background suppression results of different methods for eight IR image sequences. A1-A8 denote the 3D intensity distribution of the representative frames of the eight experimental image sequences, respectively. B1-B8 represent the 3D intensity distribution of the results of our method in the eight image sequences, respectively. C1-AC represent the 3D intensity distribution of the results of the Max-Mean method in the eight image sequences, respectively. D1-D8 represent the 3D intensity distribution of the results of Max-Median method in the eight image sequences, respectively. E1-E8 represent the 3D intensity distribution of the results of the TDLMS method in the eight image sequences, respectively. F1-F8 represent the 3D intensity distribution of the results of Kim's method in the eight image sequences, respectively. G1-G8 represent the 3D intensity distribution of the results of the 3DCF method in the eight image sequences, respectively. H1-H8 represent the 3D intensity distribution of the results of the DBM3D+GMMF method in the eight image sequences, respectively. The small targets are indicated by red ovals.**

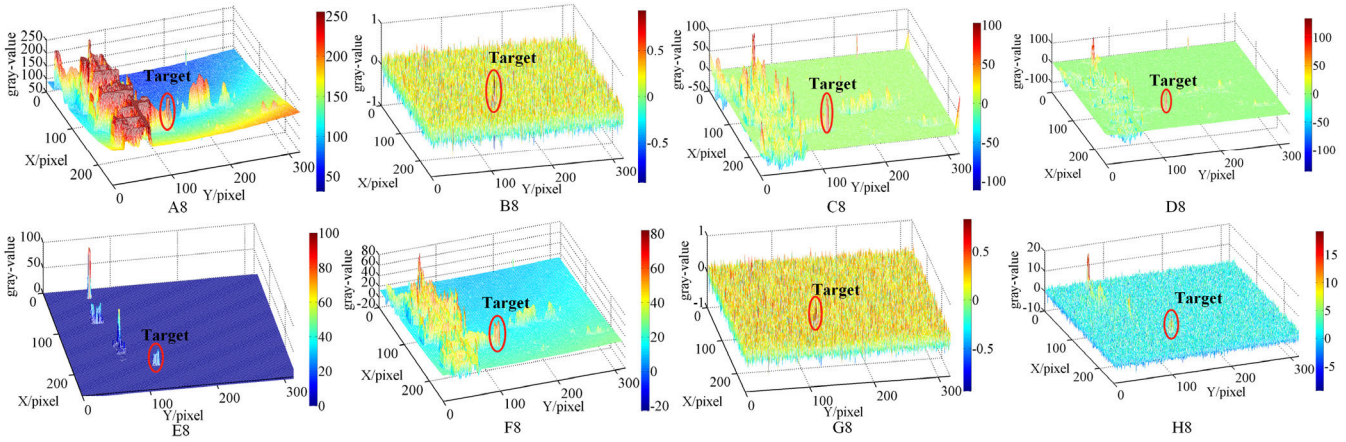

FIGURE 11. *(Continued.)* **The 3D intensity distribution of the background suppression results of different methods for eight IR image sequences. A1-A8 denote the 3D intensity distribution of the representative frames of the eight experimental image sequences, respectively. B1-B8 represent the 3D intensity distribution of the results of our method in the eight image sequences, respectively. C1-AC represent the 3D intensity distribution of the results of the Max-Mean method in the eight image sequences, respectively. D1-D8 represent the 3D intensity distribution of the results of Max-Median method in the eight image sequences, respectively. E1-E8 represent the 3D intensity distribution of the results of the TDLMS method in the eight image sequences, respectively. F1-F8 represent the 3D intensity distribution of the results of Kim's method in the eight image sequences, respectively. G1-G8 represent the 3D intensity distribution of the results of the 3DCF method in the eight image sequences, respectively. H1-H8 represent the 3D intensity distribution of the results of the DBM3D+GMMF method in the eight image sequences, respectively. The small targets are indicated by red ovals.**

TABLE 6. **The comparison results for average GSCR in different sequences.**

Methods	Seq. 1	Seq. 2	Seq. 3	Seq. 4	Seq. 5	Seq. 6	Seq. 7	Seq. 8
	$\overline{G_{SCR}}$	$\overline{G_{SCR}}$	$\overline{G_{SCR}}$	$\overline{G_{SCR}}$	$\overline{G_{SCR}}$	$\overline{G_{SCR}}$	$\overline{G_{SCR}}$	$\overline{G_{SCR}}$
Max-Mean	10.69	2.032	0.47	0.87	1.66	1.52	2.70	0.28
Max-Median	5.473	13.59	4.10	1.56	3.62	2.82	5.62	0.15
TDLMS	8.892	11.56	**32.06**	4.03	13.29	**3.02**	6.13	**1.57**
Kim's method	0.512	2.62	0.15	4.57	1.96	1.10	2.63	0.47
3DCF method	33.05	4.61	5.65	2.37	3.88	1.67	6.20	0.98
DBM3D+GMMF	26.17	22.14	1.32	0.66	2.20	0.38	3.37	0.86
Our method	**35.45**	**23.33**	6.81	**6.96**	**15.49**	1.86	**7.07**	1.33

TABLE 7. **The comparison results for average BSF in different sequences.**

Methods	Seq. 1	Seq. 2	Seq. 3	Seq. 4	Seq. 5	Seq. 6	Seq. 7	Seq. 8
	$\overline{BSF}$	$\overline{BSF}$	$\overline{BSF}$	$\overline{BSF}$	$\overline{BSF}$	$\overline{BSF}$	$\overline{BSF}$	$\overline{BSF}$
Max-Mean	8.67	6.10	6.55	6.28	5.66	5.67	7.82	3.98
Max-Median	16.98	10.92	8.89	8.69	8.52	7.66	12.88	4.68
TDLMS	24.92	31.99	21.19	30.58	30.46	22.30	28.24	20.23
Kim's method	6.55	6.32	6.36	6.34	6.23	6.13	6.62	5.58
3DCF method	74.41	89.81	80.82	80.90	83.24	92.70	65.16	164.74
DBM3D+GMMF	28.33	34.20	38.05	29.53	37.25	43.06	39.37	41.26
Our method	**213.31**	**192.22**	**106.37**	**203.48**	**223.53**	**173.21**	**83.0926**	**264.66**

has the least clutter residual and the best clutter suppression performance in these eight image sequences.

To further objectively evaluate the target signal enhancement performance and the background suppression performance of the seven methods on image sequences in different scenarios, Table 6 and Table 7 show the average G_{SCR} ($\overline{G_{SCR}}$) and average BSF ($\overline{BSF}$) of the different methods in the eight IR image sequences. The value of the G_{SCR} in Table 6 is the value obtained by using the position of the real target. Our method can be seen to have the highest $\overline{BSF}$ in all image sequences, which also indicates that our method has the best clutter suppression performance. At the same time, we can see that our method has the highest $\overline{G_{SCR}}$ in sequences 1, 2, 4, 5, and 7, which means that our method has the best target signal enhancement performance in these sequences. In addition, for sequences 3, 6, and 8, the TDLMS method has the best target signal enhancement performance and clutter suppression performance. For sequence 1 and 2, the DBM3D+GMMF method has better performance. As seen in Table 6, although we used target-like points in the process of obtaining the optimal algorithm parameters, the signals of the real targets after using the optimal algorithm parameters

TABLE 8. The average running time (seconds) of the different methods.

Method	Seq. 1	Seq. 2	Seq. 3	Seq. 4	Seq. 5	Seq. 6	Seq. 7	Seq. 8	Average
Max-Mean	1.93	1.97	1.95	1.92	1.96	1.97	1.94	1.96	1.95
Max-Median	1.82	1.84	1.86	1.85	1.86	1.86	1.82	1.82	1.84
TDLMS	12.73	13.06	13.58	12.69	12.75	13.42	12.97	13.61	13.10
Kim's method	0.95	0.91	0.98	0.90	0.89	0.93	0.88	0.89	0.92
3DCF	1.96	2.01	1.97	1.89	1.94	2.03	1.91	1.87	1.95
DBM3D+GMMF	45.03	42.17	58.12	43.45	39.08	55.32	57.04	41.87	47.76
Our method	36.97	41.18	39.86	41.23	37.75	37.87	26.32	25.82	35.87

in the eight sequences are also improved. These results prove the effectiveness of our proposed method.

According to the results of the above comparative experiments, we are able to see that our method can effectively suppress the complicated background in different scenarios while enhancing the small target signal.

To compare the computational complexity of different methods, the average running time is employed to reflect the computational performance. These comparative experiments are performed on a computer with a 2.30-GHz Intel Xeon CPU E5-2650 processor and 16-GB RAM, and the code for all algorithms are run in MATLAB R2014b. Table 8 shows the average runtime for different methods on eight IR image sequences with different backgrounds. From the table, we can see that Kim's method has the shortest average running time, and the DBM3D+GMMF method has the longest average running time of the baseline methods. Although the average running time of our method is longer than some baseline methods, it is acceptable to sacrifice a little time to maintain the high performance of the algorithm. In addition, with the development of field programmable gate array (FPGA) pipelines and the wide application of this technology, we believe that this structural design will come to offset some of the time complexity.

VII. CONCLUSION

In this paper, to improve the detection performance of dim and small targets in IR images containing high-intensity cloud clutter, a novel adaptive background suppression method is proposed. The experiments using IR images of real complex scenes have verified its advantages:

1) The proposed adaptive background suppression method can effectively suppress a background with high-intensity cloud clutter and has better background suppression performance.
2) The proposed local optimization strategy is feasible, which ensures that the proposed adaptive background suppression algorithm has the optimal parameters.

In summation, the proposed adaptive background suppression method uses the optimization algorithm to acquire the optimal algorithm parameters, which effectively improves its performance in suppressing high-intensity cloud clutter in IR images. In the future, we will try to utilize additional similar features of successive images to improve the performance of the filtering algorithm, and we will try to implement the algorithm on hardware that reduces its computational complexity.

ACKNOWLEDGMENT

The authors would like to thank the anonymous reviewers for the valuable comments and suggestions.

REFERENCES

[1] S. Matteoli, N. Acito, M. Diani, and G. Corsini, "An automatic approach to adaptive local background estimation and suppression in hyperspectral target detection," *IEEE Trans. Geosci. Remote Sens.*, vol. 49, no. 2, pp. 790–800, Feb. 2011.

[2] H. Zhang, L. Zhang, D. Yuan, and H. Chen, "Infrared small target detection based on local intensity and gradient properties," *Infr. Phys. Technol.*, vol. 89, pp. 88–96, Mar. 2018.

[3] H. Qin, J. Han, X. Yan, J. Li, H. Zhou, J. Zong, B. Wang, and Q. Zeng, "Multiscale random projection based background suppression of infrared small target image," *Infr. Phys. Technol.*, vol. 73, pp. 255–262, Nov. 2015.

[4] X. Wang, Z. Peng, D. Kong, and Y. He, "Infrared dim and small target detection based on stable multisubspace learning in heterogeneous scene," *IEEE Trans. Geosci. Remote Sens.*, vol. 55, no. 10, pp. 5481–5493, Oct. 2017.

[5] H. Ding and H. Zhao, "Adaptive method for the detection of infrared small target," *Opt. Eng.*, vol. 54, no. 11, Nov. 2015, Art. no. 113107.

[6] R. Venkateswarlu, "Max-mean and Max-median filters for detection of small targets," *Proc. SPIE*, vol. 3809, Jul. 1999, pp. 74–83.

[7] P.-Y. Lv, S.-L. Sun, C.-Q. Lin, and G.-R. Liu, "Space moving target detection and tracking method in complex background," *Infr. Phys. Technol.*, vol. 91, pp. 107–118, Jun. 2018.

[8] Y. Gu, C. Wang, B. Liu, and Y. Zhang, "A kernel-based nonparametric regression method for clutter removal in infrared small-target detection applications," *IEEE Geosci. Remote Sens. Lett.*, vol. 7, no. 3, pp. 469–473, Jul. 2010.

[9] T.-W. Bae and K.-I. Sohng, "Small target detection using bilateral filter based on edge component," *J. Infr., Millim., Terahertz Waves*, vol. 31, pp. 735–743 Jun. 2010.

[10] S. Kim, Y. Yang, J. Lee, and Y. Park, "Small target detection utilizing robust methods of the human visual system for IRST," *J. Infr., Millim., Terahertz Waves*, vol. 30, no. 9, pp. 994–1011, Sep. 2009.

[11] X. Shao, H. Fan, G. Lu, and J. Xu, "An improved infrared dim and small target detection algorithm based on the contrast mechanism of human visual system," *Infr. Phys. Technol.*, vol. 55, no. 5, pp. 403–408, Sep. 2012.

[12] A. Tzannes and D. Brooks, "Temporal filters for point target detection in IR imagery," *Proc. SPIE*, vol. 3061, Apr. 1997, pp. 508–520.

[13] A. L. Da Cunha, J. Zhou, and M. N. Do, "The nonsubsampled contourlet transform: Theory, design, and applications," *IEEE Trans. Image Process.*, vol. 15, no. 10, pp. 3089–3101, Oct. 2006.

[14] J. Gong, Y. Zhang, Q. Hou, W. He, H. Guan, and W. Zhang, "Background suppression for cloud clutter using temporal difference projection," *Infr. Phys. Technol.*, vol. 64, pp. 66–72, May 2014.

[15] E. Lim, S. Deshpande, C. Chan, and R. Venkateswarlu, "Dim point target detection in IR imagery using multistage IIR filter," *Proc. SPIE*, vol. 4025, Apr. 2000, pp. 194–202.

[16] J. Silverman, J. M. Mooney, and C. E. Caefer, "Temporal filters for tracking weak slow point targets in evolving cloud clutter," *Infr. Phys. Technol.*, vol. 37, no. 6, pp. 695–710, Oct. 1996.

[17] L. Yang, J. Yang, and K. Yang, "Adaptive detection for infrared small target under sea-sky complex background," *Electron. Lett.*, vol. 40, no. 17, pp. 1083–1085, Aug. 2004.

[18] L. Lei and Q. ShiRu, "A novel approach of infrared small weak target detection based on an improved nonsubsampled contourlet transform," in *Proc. IEEE Int. Conf. Signal Process., Commun. Comput. (ICSPCC)*, Xi'an, China, Sep. 2011, pp. 1–4.
[19] Y.-Q. Sun, J.-W. Tian, and J. Liu, "Background suppression based-on wavelet transformation to detect infrared target," in *Proc. Int. Conf. Mach. Learn. Cybern.*, Canton, China, Aug. 2005, pp. 4611–4615.
[20] A. Buades, B. Coll, and J.-M. Morel, "A non-local algorithm for image denoising," in *Proc. IEEE Comput. Soc. Conf. Comput. Vis. Pattern Recognit. (CVPR)*, San Diego, CA, USA, Jul. 2005, pp. 60–65.
[21] L. Genin, F. Champagnat, G. Le Besnerais, and L. Coret, "Point object detection using a NL-means type filter," in *Proc. 18th IEEE Int. Conf. Image Process.*, Brussels, Belgium, Sep. 2011, pp. 3533–3536.
[22] L. Genin, F. Champagnat, and G. Le Besnerais, "Background first- and second-order modeling for point target detection," *Appl. Opt.*, vol. 51, no. 31, p. 7701, Nov. 2012.
[23] K. Dabov, A. Foi, V. Katkovnik, and K. Egiazarian, "Image denoising by sparse 3-D transform-domain collaborative filtering," *IEEE Trans. Image Process.*, vol. 16, no. 8, pp. 2080–2095, Aug. 2007.
[24] M. Lebrun, "An analysis and implementation of the BM3D image denoising method," *Image Process. Line*, vol. 2, pp. 175–213, Sep. 2012.
[25] J. Hu, Y. Yu, and F. Liu, "Small and dim target detection by background estimation," *Infr. Phys. Technol.*, vol. 73, pp. 141–148, Nov. 2015.
[26] H. Pan, T.-Z. Huang, and T. Ma, "Two-step group-based adaptive soft-thresholding algorithm for image denoising," *Optik*, vol. 127, no. 1, pp. 503–509, Jan. 2016.
[27] D. L. Donoho and I. M. Johnstone, "Ideal spatial adaptation by wavelet shrinkage," *Biometrika*, vol. 81, no. 3, pp. 425–455, Sep. 1994.
[28] D. L. Donoho, "De-noising by soft-thresholding," *IEEE Trans. Inf. Theory*, vol. 41, no. 3, pp. 613–627, May 1995.
[29] T.-J. Su, J.-C. Cheng, and C.-J. Yu, "An adaptive channel equalizer using self-adaptation bacterial foraging optimization," *Opt. Commun.*, vol. 283, no. 20, pp. 3911–3916, Oct. 2010.
[30] S. Gholami-Boroujeny and M. Eshghi, "Non-linear active noise cancellation using a bacterial foraging optimisation algorithm," *IET Signal Process.*, vol. 6, no. 4, p. 364, 2012.
[31] M. K. Ahirwal, A. Kumar, and G. K. Singh, "EEG/ERP adaptive noise canceller design with controlled search space (CSS) approach in cuckoo and other optimization algorithms," *IEEE/ACM Trans. Comput. Biol. Bioinformatics*, vol. 10, no. 6, pp. 1491–1504, Nov. 2013.
[32] X. R. Tong, "Research on the white noise suppression by adaptive filtering of genetic algorithm," *Appl. Mech. Mater.*, vols. 155–156, pp. 989–994, Feb. 2012.
[33] R. Eberhart, and J. Kennedy, "A new optimizer using particle swarm theory," in *Proc. 8th Int. Symp. Micromach. Hum. Sci.*, Nagoya, Japan, Oct. 1995, pp. 39–43.
[34] J. Kennedy and R. C. Eberhart, "Particle swarm optimization," in *Proc. IEEE Int. Conf. Neural Netw.*, Piscataway, NJ, USA, Dec. 1995, pp. 1942–1948.
[35] J. J. Liang, A. K. Qin, P. N. Suganthan, and S. Baskar, "Comprehensive learning particle swarm optimizer for global optimization of multimodal functions," *IEEE Trans. Evol. Comput.*, vol. 10, no. 3, pp. 281–295, Jun. 2006.
[36] C. Yue, B. Qu, and J. Liang, "A multiobjective particle swarm optimizer using ring topology for solving multimodal multiobjective problems," *IEEE Trans. Evol. Comput.*, vol. 22, no. 5, pp. 805–817, Oct. 2018.
[37] G. G. Bhutada, R. S. Anand, and S. C. Saxena, "PSO-based learning of sub-band adaptive thresholding function for image denoising," *Signal, Image Video Process.*, vol. 6, no. 1, pp. 1–7, Mar. 2012.
[38] V. Soni, A. Kumar, G. K. Singh, and A. K. Bhandari, "Improved sub-band adaptive thresholding function for denoising of satellite image based on evolutionary algorithms," *IET Signal Process.*, vol. 7, no. 8, pp. 720–730, Oct. 2013.
[39] U. Mahbub, C. Shahnaz, and S. Anowarul Fattah, "An adaptive noise cancellation scheme using particle swarm optimization algorithm," in *Proc. Int. Conf. Commun. Control Comput. Technol.*, Ramanathapuram, India, Oct. 2010, pp. 683–686.
[40] L. Sheng, W. Bangmin, and Z. Lanyong, "Intelligent adaptive filtering algorithm for electromagnetic-radiation field testing," *IEEE Trans. Electromagn. Compat.*, vol. 59, no. 6, pp. 1765–1780, Dec. 2017.
[41] M. K. Ahirwal, A. Kumar, and G. K. Singh, "Adaptive filtering of EEG/ERP through noise cancellers using an improved PSO algorithm," *Swarm Evol. Comput.*, vol. 14, pp. 76–91, Feb. 2014.
[42] T. Ma, Z. Shi, J. Yin, Y. Liu, B. Xu, and C. Zhang, "Rectilinear-motion space inversion-based detection approach for infrared dim air targets with variable velocities," *Opt. Eng.*, vol. 55, no. 3, Mar. 2016, Art. no. 033102.
[43] M. Clerc and J. Kennedy, "The particle swarm–explosion, stability, and convergence in a multidimensional complex space," *IEEE Trans. Evol. Comput.*, vol. 6, no. 1, pp. 58–73, 2002.
[44] K. Yu, L. While, M. Reynolds, X. Wang, J. J. Liang, L. Zhao, and Z. Wang, "Multiobjective optimization of ethylene cracking furnace system using self-adaptive multiobjective AC-based optimization," *Energy*, vol. 148, pp. 469–481, Apr. 2018.
[45] J. J. Liang, X. P. Zhu, C. T. Yue, Z. H. Li, and B. Y. Qu, "Performance analysis on knee point selection methods for multi-objective sparse optimization problems," in *Proc. IEEE Congr. Evol. Comput. (CEC)*, Rio de Janeiro, Brazil, Jul. 2018, pp. 1–8.
[46] X. Ren, J. Wang, T. Ma, K. Bai, M. Ge, and Y. Wang, "Infrared dim and small target detection based on three-dimensional collaborative filtering and spatial inversion modeling," *Infr. Phys. Technol.*, vol. 101, pp. 13–24, Sep. 2019.
[47] J. Gao, Z. Lin, and W. An, "Infrared small target detection using a temporal variance and spatial patch contrast filter," *IEEE Access*, vol. 7, pp. 32217–32226, 2019.
[48] Q. Zhang and H. Li, "MOEa/D: A multiobjective evolutionary algorithm based on decomposition," *IEEE Trans. Evol. Comput.*, vol. 11, no. 6, pp. 712–731, Dec. 2007.
[49] J. J. Liang, C. T. Yue, and B. Y. Qu, "Multimodal multi-objective optimization: A preliminary study," in *Proc. IEEE Congr. Evol. Comput. (CEC)*, Jul. 2016, pp. 2454–2461.
[50] C. Gao, L. Wang, Y. Xiao, Q. Zhao, and D. Meng, "Infrared small-dim target detection based on Markov random field guided noise modeling," *Pattern Recognit.*, vol. 76, pp. 463–475, Apr. 2018.
[51] H. Deng, X. Sun, M. Liu, C. Ye, and X. Zhou, "Entropy-based window selection for detecting dim and small infrared targets," *Pattern Recognit.*, vol. 61, pp. 66–77, Jan. 2017.
[52] C. Yue, J. Liang, B. Qu, Y. Han, Y. Zhu, and O. D. Crisalle, "A novel multiobjective optimization algorithm for sparse signal reconstruction," *Signal Process.*, vol. 167, Feb. 2020, Art. no. 107292.
[53] X. Y. Ren, J. Wang, and T. L. Ma, "Review on infrared dim and small target detection technology," *J. Zhengzhou Univ. (Nat. Sci. Ed.)*, to be published, doi: 10.13705/j.issn.1671-6841.2019557.

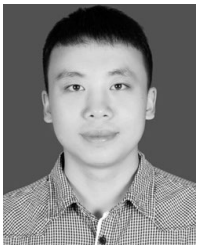

XIANGYANG REN (Student Member, IEEE) received the B.E. degree from the College of Information and Business, Zhongyuan University of Technology, Zhengzhou, China, in 2013, and the M.S. degree from the Kunming University of Science and Technology, Kunming, China, in 2016. He is currently pursuing the Ph.D. degree with the Zhengzhou University. His current research interests include IR dim and small target detection, and multiobjective optimization.

JIE WANG received the B.E. degree from Jinan Univercity, Jinan, China, the M.S. degree from Chongqing University, Chongqing, China, and the Ph.D. degree from Zhengjiang University, Hangzhou, China. He is currently a Professor with the School of Electrical Engineering, Zhengzhou University, China. His main research interests are image and video signal processing, intelligent control, and evolutionary computation.

TIANLEI MA received the B.E. degree in automation from Zhengzhou University, Zhengzhou, China, in 2010, and the Ph.D. degree from the University of Chinese Academy of Sciences, Beijing, China. He is currently an Associate Professor with the School of Electrical Engineering, Zhengzhou University. His current research interests include IR dim target detection, image processing, and pattern recognition.

CAITONG YUE (Student Member, IEEE) received the B.E. degree from Zhengzhou University, Zhengzhou, China, in 2014, where he is currently pursuing the Ph.D. degree. His current research interests include evolutionary computation, swarm intelligence, multiobjective optimization, and sparse optimization.

KE BAI received the B.E. and M.S. degrees from the North China University of Water Resources and Electric Power, Zhengzhou, China, in 2013 and 2016, respectively. He is currently pursuing the Ph.D. degree with Zhengzhou University. His current research interests include image processing, image deblurring, and sparse optimization.